Title

Observed and Simulated Sensitivities of Spring Greenup to Preseason Climate in Northern Temperate and Boreal Regions

Journal

Journal of Geophysical Research Biogeosciences, 123(1)

ISSN

2169-8953

Authors

Xu, Xiyan
Riley, William J
Koven, Charles D
et al.

Publication Date

2018

DOI

10.1002/2017jg004117

Peer reviewed

Observed and Simulated Sensitivities of Spring Greenup to Preseason Climate in Northern Temperate and Boreal Regions

Xiyan Xu[1,2] , William J. Riley[2] , Charles D. Koven[2] , and Gensuo Jia[1]

[1] Key Laboratory of Regional Climate-Environment for Temperate East Asia, Institute of Atmospheric Physics, Chinese Academy of Sciences, Beijing, China, [2] Climate and Ecosystem Sciences Division, Lawrence Berkeley National Laboratory, Berkeley, CA, USA

Correspondence to: G. Jia, jiong@tea.ac.cn

Abstract

Vegetation phenology plays an important role in regulating land-atmosphere energy, water, and trace-gas exchanges. Changes in spring greenup (SG) have been documented in the past half-century in response to ongoing climate change. We use normalized difference vegetation index generated from NOAA's advanced very high resolution radiometer data in the Global Inventory Modeling and Monitoring Study project over the 1982–2005 period, coupled with climate reanalysis (Climate Research Unit-National Centers for Environmental Prediction) to investigate the SG responses to preseason climate change in northern temperate and boreal regions. We compared these observed responses to the simulated SG responses to preseason climate inferred from the Earth system models (ESMs) participating in the Coupled Model Intercomparison Project Phase 5 (CMIP5) over 1982–2005. The observationally inferred SG suggests that there has been an advance of about 1 days per decade between 1982 and 2005 in the northern midlatitude to high latitude, with significant spatial heterogeneity. The spatial heterogeneity of the SG advance results from heterogeneity in the change of the preseason climate as well as varied vegetation responses to the preseason climate across biomes. The SG to preseason temperature sensitivity is highest in forests other than deciduous needleleaf forests, followed by temperate grasslands and woody savannas. The SG in deciduous needleleaf forests, open shrublands, and tundra is relatively insensitive to preseason temperature. Although the extent of regions where the SG is sensitive to preseason precipitation is smaller than the extent of regions where the SG is sensitive to preseason temperature, the biomes that are more sensitive to temperature are also more sensitive to precipitation, suggesting the interactive control of temperature and precipitation. In the mean, the CMIP5 ESMs reproduced the dominant latitudinal preseason climate trends and SG advances. However, large biases in individual ESMs for the preseason period, climate, and SG sensitivity imply needed model improvements to climate prediction and phenological process parameterizations.

1 Introduction

Vegetation phenology is the study of the seasonal life cycle of plants controlled by seasonal and interannual climate change. Vegetation phenology influences land-atmosphere exchanges of energy, water, and trace gases. A shift in phenological timing has been documented in the past half-century in response to ongoing climate change (Gordo & Sanz, 2010; Menzel, Sparks, et al., 2006; Shen, Tang, et al., 2014). The 5th Assessment Report (Settele et al., 2014) of the Intergovernmental Panel on Climate Change synthesized multiple studies to conclude that spring greenup (SG), the time at which plants begin to grow leaves in northern midlatitude and high latitude, has advanced at a rate of between 1.1 and 5.2 days per decade over different periods and regions.

The patterns of SG shifts have large spatial and temporal heterogeneity. According to the European Phyto-phenological data set during 1951–1998, SG was delayed by up to 3 days per decade in east Europe, whereas in central and western Europe, SG advanced at the rate of >5 days per decade (Ahas et al., 2002). The SG advance rate based on the European Phyto-phenological data set over 1951–1998 in central and western Europe is approximately equivalent to the Europe-wide mean advances during 1982–2000, as derived from Pathfinder Advanced Very High Resolution Radiometer Land Normalized Difference Vegetation Index Data (Stöckli & Vidale, 2004). In East Asia, SG has advanced >7 days per decade over 1982–2000, as determined by Global Inventory Modeling and Monitoring Study (GIMMS) NDVI data (Chen et al., 2005; Jeong et al., 2009; Piao et al., 2006). In North America, the advance of SG was up to 6 days per decade over 1985–1999, based on Pathfinder AVHRR Land NDVI (De Beurs & Henebry, 2005). Analysis of GIMMS NDVI demonstrated that although the Northern Hemisphere has experienced an SG advance of 3–4 days per decade from 1982 to 1999, the advance was no longer present during 2000–2008 (Jeong et al., 2011).

Shifts in the SG are the result of dynamic plant responses to climate variability and change, and the shifts vary among vegetation types and species. Temperature has long been recognized as the dominant factor that alters SG, and that its effects differ between plant species (Gordo & Sanz, 2010; Seghieri et al., 2012). The records of tree SG over 100 years from England (Thompson & Clark, 2008) and flowering in the northeastern U.S. (Miller-Rushing & Primack, 2008) have chronicled advances of 3–8 days for each 1°C increase in air temperature over the 1 or 2 months preceding the SG or flowering. European larch in northern Italy Alpine regions has advanced at a rate of 7 days per °C increase in spring air temperature (Busetto et al., 2010). The response of SG in temperate China varied from advances of 9.7 days to delays of 6.3 days with a mean advance of 1.2 days per °C in preseason temperature increase, according to different methods to evaluate SG with AVHRR GIMMS-NDVI3g data (Cong et al., 2013). The vegetation types with earlier mean SG in lower latitude are more sensitive to temperature increases and show larger advances over the historical period (Shen, Tang, et al., 2014), and 88% of the latitudinal variability in the SG

trend can be explained by preseason temperature (Shen et al., 2015). In addition to temperature control, a weaker temperature sensitivity of SG for some vegetation species can be attributed to changes in water availability. Delayed SG in response to increased air temperature has been reported in East Asia semiarid regions due to reduced precipitation (Shen et al., 2011; Yu et al., 2003). In the boreal forest, the precipitation influence on SG has been shown not to be significant, except that heavy snowfall can cause delays in SG (Borner et al., 2008; Shutova et al., 2006). In high-latitude and high-altitude regions, thin and early melting snowpack may cause frost damage to vegetation (Inouye, 2008; Wipf et al., 2006). But most likely, an early snowmelt reflects a warmer snowmelt season, which is consistent with temperature controls on SG (Peng et al., 2013). The various SG responses to environmental factors across regions and biomes make it one of the most complicated issues in modeling ecosystem processes.

Accurate representation of phenological processes in climate models is essential to predict mass and energy exchange between land and the atmosphere and the response of surface exchange processes to climate change. Climate models that include dynamic leaf phenology generally use thermal forcing or combined thermal forcing and chilling to predict the timing of SG, in which SG occurs when the state of forcing (S (t)) reaches a critical forcing unit summation (F). In the spring warming approach, accumulated forcing is calculated dependent on the starting date of forcing accumulation and air temperature (Sarvas, 1972). The sequential approach assumes a similar forcing accumulation, but the date of forcing accumulation begins when accumulated chilling units reach a critical threshold (Hänninen, 1990; Kramer, 1994). The alternating approach assumes that the chilling and forcing take turns accumulating from an initial start date of a single base temperature, in which the critical temperature threshold for SG depends on accumulated chilling such that with more chilling, the larger the forcing accumulation that is required for greenup (Cannell & Smith, 1983). Alternate approaches exist: e.g., Kikuzawa (1995) predicted leaf phenology based on a carbon cost and benefit analysis and nutrient availability. In the current generation of Earth system models (ESMs), which couple land surface and atmospheric processes, the seasonality of ecosystem processes that control vegetation phenology is represented by using the spring warming approaches applied to different plant functional types (PFTs), although the prescription of parameters and PFT classifications vary among the models (Text S1). Multiple studies indicate that land surface schemes used in current ESMs do not place sufficient emphasis on accurately modeling seasonality of ecosystem processes that affect vegetation phenology (Anav et al., 2013; Richardson et al., 2012).

In order to quantitatively evaluate the ESMs in modeling spring vegetation phenology and its responses to climate factors, we compare modeled spring phenology with satellite-inferred spring phenology in the northern temperate and boreal regions over 1982–2005. The main objectives of this work are to

explore, across biomes and in observations and ESMs, (1) the preseason when climate exerts significant control on the SG, (2) the sensitivity of the SG to preseason temperature and precipitation, and (3) historical trends in the SG and their associated climate controls. Data and methods are described in section 2. The results of the analysis of the preseason climate that regulates the SG and sensitivities of the SG to preseason climate are presented in section 3. Discussions and conclusions are given in sections 4 and 5, respectively.

2 Data and Method

2.1 Study Area

We restrict our analysis to north of 30°N, where temperate and boreal vegetation dominate, since that is the region where phenology is expected to be most strongly controlled by the annual cycle of temperature and moisture availability. We also limit our analysis to south of 80°N, due to the limited extent of terrestrial ecosystems beyond this latitude.

2.2 Earth System Models

We analyzed twentieth century historical simulations from ESMs participating in CMIP5 (Taylor et al., 2012). These coupled land-atmosphere-ocean simulations were forced by time-varying greenhouse gases, aerosols, and land use change. We used the first ensemble member from 11 ESMs (Table 1) to infer SG from monthly leaf area index (LAI) between 1982 and 2005, which we chose to be consistent with the period of GIMMS NDVI data. To assess phenological control by climate, we needed daily meteorology from the ESMs, as monthly meteorology was too coarse to accurately infer sensitivity. Daily climate data (i.e., surface air temperature (tas) and daily precipitation (pr)) were available for 5 of the 11 ESMs.

Table 1
The CMIP5 Models Participating in Phenology Analyses

	List of ESMs (only the first ensemble member was used)	
	Model name	Institution
1	BCC-CSM1	Beijing Climate Center (BCC), China Meteorological Administration, China
2	BNU-ESM	College of Global Change and Earth System Science, Beijing Normal University
3	CanESM2	Canadian Centre for Climate Modeling and Analysis
4	CCSM4[a]	NCAR (National Center for Atmospheric Research) Boulder, CO, USA
5	GFDL-ESM2G	Geophysical Fluid Dynamics Laboratory
6	HadGEM2-CC[a]	Met Office Hadley Centre, Fitzroy Road, Exeter, Devon, EX1 3 PB, UK
7	INM-CM4[a]	INM (Institute for Numerical Mathematics, Moscow, Russia)
8	IPSL-CM5A-LR[a]	IPSL (Institut Pierre Simon Laplace, Paris, France)
9	MIROC-ESM	JAMSTEC (Japan Agency for Marine-Earth Science and Technology, Kanagawa, Japan), AORI (Atmosphere and Ocean Research Institute, The University of Tokyo, Chiba, Japan), and NIES (National Institute for Environmental Studies, Ibaraki, Japan)
10	MPI-ESM-LR[a]	Max Planck Institute for Meteorology
11	NorESM1-M	Norwegian Climate Centre

[a]The ESMs with daily air temperature and precipitation outputs that we used to analyze the phenology response to climate.

2.3 Climate Reanalysis

The daily mean temperature (T_m) and cumulative precipitation (P_c) are calculated from 6-hourly, half-degree resolution CRU-NCEP (Climate

Research Unit-National Centers for Environmental Prediction) v6 reanalysis to analyze the preseason climate associated with SG derived from GIMMS NDVI. The CRU-NCEP v6 data set, recently extended to 2014, is a combination of CRU TS v3.2 0.5° × 0.5° monthly climatology and NCEP reanalysis 2.5° × 2.5° with 6 h time step available in near real time (http://forge.ipsl.jussieu.fr/orchidee/wiki/Documentation/Forcings).

2.4 Satellite Data

We used the latest version of the AVHRR instrument onboard the NOAA satellite series NDVI data set (GIMMS3g), which spans the period from July 1981 to December 2013 and has a spatial resolution of 1/12° and bimonthly temporal resolution (Pinzon & Tucker, 2014). We regridded GIMMS NDVI3g data to half-degree resolution using a bilinear method to match the spatial resolution of the CRU-NCEP reanalysis. We used the period 1982–2005 to match that of the model outputs.

In order to analyze the phenology and its response to climate across biomes, we used global mosaics of collection 6 Moderate Resolution Imaging Spectroradiometer (MODIS) data products (MCD12Q1) in the International Geosphere-Biosphere Programme (IGBP) classification of land cover types with spatial resolution of 0.5° × 0.5° to mask the model and satellite-based SG results. The global mosaics of MCD12Q1 with geographic coordinates of latitude and longitude on the WGS 1984 coordinate reference system (EPSG: 4326) (Channan et al., 2014) were reprojected from standard MCD12Q1 with 500 m resolutions (Friedl et al., 2010). We used the IGBP land cover classification for nine biomes in 2012 (Table S1): evergreen needleleaf forest, deciduous needleleaf forest, deciduous broadleaf forest, mixed forest, open shrublands, woody savannas, grassland, permanent wetland, and cropland. We distinguish the grassland to the north of 60°N, which is more likely to be tundra, from grassland in the temperate south due to their expected differences in climate and controls on phenology (Figure S1 in the supporting information).

2.5 Determination of SG and Preseason Climate

We determined the preseason following the method of Shen, Tang, et al. (2014), but with a different climate reanalysis product and method for calculating the SG.

2.5.1 SG and Mean SG

We first apply a piecewise logistic method (Zhang et al., 2003) to fit the temporal variation of vegetation index data (LAI or NDVI) to vegetation growth:

$$y(t) = \frac{c}{1 + e^{a+bt}} + d \quad (1)$$

where t is time in days, $y(t)$ is the vegetation index at time t, a and b are fitting parameters, $c + d$ is the maximum vegetation index value, and d is

the initial background vegetation index, usually the minimum vegetation index value preceding the growing season. The SG is identified as the Julian date at which the rate of change in the vegetation growth ($y(t)$) is maximum, which is the maximum of the second derivative of equation 1. The long-term mean SG (MSG) in each pixel is averaged over the analysis years. The piecewise logistic method is applied to CMIP5 LAI outputs and GIMMS NDVI products. The LAI and NDVI-derived SGs are comparable because NDVI and LAI exhibit strong linear relationship for grass (Fan et al., 2009) and shrubs (Green et al., 1997) and in the leaf production period for forest (Wang et al., 2005). For the pixels with multiple growth cycles in a year, we applied this piecewise logistic method to the first cycle, so that SG is the Julian date at which the second derivative of $y(t)$ is maximum for the first time in a year.

2.5.2 Preseason Period and Preseason Climate

We hypothesize that the temperature and precipitation variability in the preseason period control phenology in different ways, which include different periods of sensitivity for the two variables. Thus, we calculate the preseason periods separately for temperature (P_T) and precipitation (P_P) to indicate the difference in temperature and precipitation controls on spring phenology. The T_m and P_c are calculated during the respective preseason periods. Negative interannual correlation between (1) preseason temperature and SG and (2) preseason precipitation and SG are used to screen the data. A preseason calculation is only made for pixels in which the correlation between SG and T_m (and P_c) is negative. The preseason climate (T_m and P_c) in each pixel is calculated in the period preceding the MSG from 15 to 120 days with an increment of 3 days. Because we expect the relative variation in precipitation to be more relevant than absolute values in determining phenology, we use the relative variation of cumulative precipitation in percentage (%) of precipitation change instead of the absolute cumulative precipitation variation in millimeter (mm). We detrended the calculated T_m and $P_c$over the historical period. For each period preceding MSG for a given pixel, we calculated the Pearson's correlation coefficients (PCC) between SG and T_m (and P_c). We defined the period with the most negative correlation between SG and T_m (and P_c) as the preseason for temperature control, P_T (and preseason for precipitation control, P_P). We used daily meteorology from the CRU-NCEP to determine the SG and MSG for observations, and daily ESM output of temperature and precipitation to determine the SG and MSG for the ESMs.

2.5.3 SG Shift and SG Response to Preseason Climate

We applied linear regression to the SG time series in each pixel to obtain the SG trend over 1982–2005 for ESM- and NDVI-based SG. We analyzed the response of SG to preseason climate by calculating linear regressions between SG and T_m (and P_c). We also excluded the SG response to preseason climate in pixels where no significant relationship was found (i.e., $p$value > 0.1). We bilinearly interpolated the model simulated SG and response of SG

to preseason climate with different model resolutions to 0.5° × 0.5°, in order to calculate the zonal mean SG and response of SG to preseason climate across IGBP land cover types.

3 Results

3.1 Observed and Modeled SG Shift

Most ESMs predicted SG shifts in the range of ±5 days per decade in the Northern Hemisphere, with large spatial heterogeneity (Figure 1). Most ESMs, except Beijing Climate Center Climate System Model version 1 (BCC-CSM1), Geophysical Fluid Dynamics Laboratory Earth System Model version 2 with Generalized Ocean Layer Dynamics (GOLD) component (GFDL-ESM2G), and Norwegian Earth System Model 1 - medium resolution (NorESM1-M) (Figures 1b, 1f, and 1l), predicted advanced the SG north of the midlatitudes, although the ESMs tended to predict larger SG advances than those from the GIMMS retrievals (Figure 1a). The most significant GIMMS-derived advances occurred in western Europe, and a similar response is also predicted by the Beijing Normal University Earth System Model (BNU-ESM), Canadian Earth System Model version 2 (CanESM2), Model for Interdisciplinary Research on Climate Earth System Model (MIROC-ESM), and Max-Planck-Institut-Earth System Model Low Resolution (MPI-ESM-LR) ESMs (Figures 1c, 1d, 1j, and 1k).

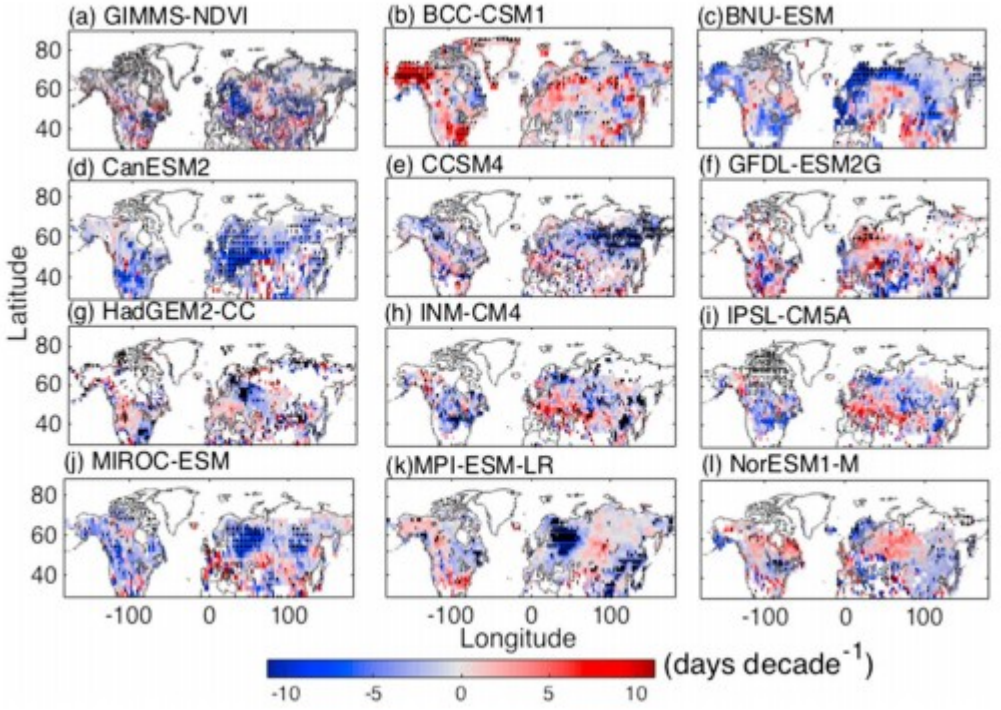

Figure 1

Phenology shift for the spring greenup (SG) in observations (GIMMS) and ESMs over the period 1982–2005. The black dot mask indicates significant trend ($p < 0.1$).

The GIMMS-derived zonal mean SG advances throughout most of the 35–80°N latitude range (Figure 2a). Although the individual model predictions show a wide spread, the mean SG shift of the multimodel mean approximately corresponds to the GIMMS-derived record. North of the midlatitude to high-latitude zone (45–80°N), the GIMMS-derived SG shift is −0.9 ± 0.5 days per decade and the ESM mean is −1.0 ± 0.6 days per decade. In contrast to the multimodel mean, the GIMMS-derived zonal mean indicates significant SG delays south of 34°N. The spatial correlation between the ESM- and GIMMS-derived predictions above 45°N is highest for CanESM2 ($r = 0.57$, $p < 0.01$; although it has one of the highest magnitude biases of all ESMs between about 35 and 60°N), followed by MPI-ESM-LR ($r = 0.33$, $p < 0.01$).

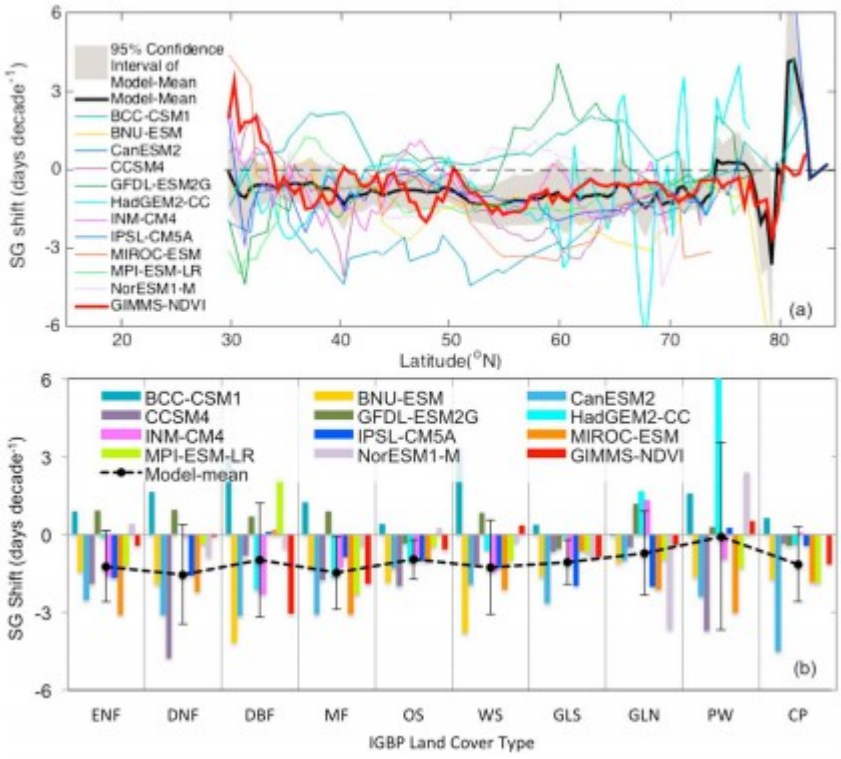

Figure 2

Spring greenup (SG) shift in observations (GIMMS) and CMIP5 ESMs. (a) SG changes for the zonal mean and (b) SG changes for IGBP land cover types. The error bars on the model mean in Figure 2b are the standard deviation of SG shift for each ESM prediction. The numbers of pixels that were used to calculate the biome-scale shift are shown in Table S2.

When we isolate changes in the SG shift to each IGBP biome classification, GIMMS shows that the SG advances in 8 of the 10 biomes (Figure 2b). However, in woody savannas and permanent wetlands, GIMMS suggests small SG delays (<1 day per decade). The GIMMS-derived SG indicates that the deciduous broadleaf forest biome has experienced the largest SG advance (3.1 days per decade) followed by those of mixed forests (1.9 days per decade), croplands (1.2 days per decade), temperate grasslands (0.9

days per decade), and open shrublands (0.6 days per decade), while the SG advances in other biomes are within ±0.5 days per decade.

Most ESMs predicted that the SG advances across most biomes, except BCC-CSM1 and GFDL-ESM2G. The multimodel mean SG advances across biomes are in the range of 0.7–1.6 days per decade. However, considerable variability within a given model and across a given biome are evident, including a few ESMs that predict a larger than observed SG advance in certain biomes, e.g., 4.8 days per decade in deciduous needleleaf forests and 3.7 days per decade in permanent wetlands by Community Climate System Model version 4 (CCSM4), 4.2 days per decade in deciduous broadleaf forests and 3.8 days per decade in woody savannas by BNU-ESM, 3.1 days per decade in deciduous needleleaf forests and mixed forests, 3.2 days per decade in deciduous broadleaf forests, and 4.5 days per decade in croplands by CanESM2. The SG shift across biomes predicted by Hadley Centre Global Environmental Model version 2 Carbon Cycle (HadGEM2-CC) is the best correlated to that of GIMMS ($r = 0.62$, $p = 0.15$), followed by CanESM2 ($r = 0.41$, $p = 0.25$), Institute of Numerical Mathematics Coupled Model version 4 (INM-CM4) ($r = 0.38$, $p = 0.28$), BNU-ESM ($r = 0.31$, $p = 0.39$), and NorESM1-M ($r = 0.20$, $p = 0.58$). The interbiome SG shifts predicted by BCC-CSM1, CCSM4, GFDL-ESM2G, Institut Pierre-Simon Laplace Coupled Model version 5A (IPSL-CM5A), MIROC-ESM, and MPI-ESM-LR are negatively correlated with GIMMS-derived values.

3.2 Observed Preseason Correlations With the SG

Because the CMIP5 ESMs are coupled land-atmosphere-ocean models, they differ from the historical record and each other both in physical process representation and in internal dynamics. We therefore examined the correlation between phenological timing and meteorology to assess whether the physics correlation between the ESMs and observations is consistent. In the northern hemisphere, the P_T is usually within 2 months of the SG (43 ± 30 days; Figure 3a). The P_T in the north of central Alaska and Canada and the south of Asia exceeds 3 months. The mean temperature during The P_T (T_m) shows strong spatial heterogeneity; however, in general, the higher the latitude the lower is T_m (Figure 3b). Moreover, the high-altitude region in south Asia shows a lower T_m there than in surrounding regions in the same latitudes. The Russian Far East and the northern North America boreal zone, from Alaska to the Hudson Bay, has the coldest P_T with a T_m lower than −25°C, while the southeast of the United States and South Asia experienced the warmest P_T ($T_m > 12$°C). The lower T_m at high altitudes is most remarkable in the Tibetan Plateau, where the T_m is more than 20°C lower than the other regions in the same latitude. The correlation between the $T_m$and SG indicates that the T_m control on SG is most significant over 45–70°N, where 65.3% of the pixels have PCC greater than 0.3 (Figure 3c). About 76.6% of the pixels with valid SG shift show a warming trend over the 1982–2005 period, in which 24.4% of the P_T warming is greater than 0.1°C yr^{-1} and 66.7% of the pixels with a warming trend occur in Eurasia (Figure

3d). The cooling trend occurs in the east of the Baltic Sea and the Great Plains of North America, in which about 13.2% of the pixels have cooling trend greater than 0.1°C yr^{-1}.

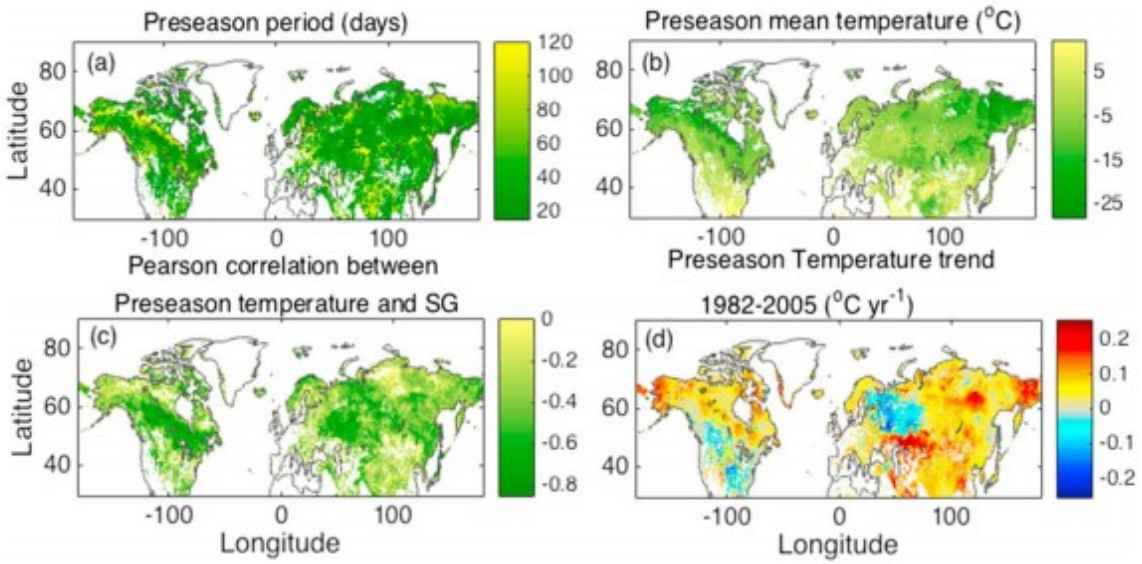

Figure 3

CRU-NCEP preseason mean temperature corresponding to GIMMS SG: (a) the duration of the preseason period of temperature control (P_T), (b) the mean temperature in P_T (T_m), (c) the PCC between T_m and SG, and (d) the T_m trend over the 1982–2005 period.

The fraction of the northern midlatitude to high-latitude land surface with preseason precipitation control is less than that for temperature control. The SG preseason period for precipitation (P_P) is longer than P_T, with the mean period of 59 ± 30 days (Figure 4a). The pixels (84.2%) with valid P_P have a P_c less than 30 mm. Only 6.8% of the pixels have a P_c over 150 mm, which are mainly distributed in the east of North America (Figure 4b). The correlation between the SG and P_c is much lower than that between the T_m and SG in most pixels. Only 28.2% of the pixels have P_c-SG correlations higher than 0.3. The P_c control on SG is relatively stronger in the northeast of the Mediterranean Sea and east of the Baltic Sea (Figure 4c) where P_c increases between 1982 and 2005 (Figure 4d); the stronger control is consistent with expectations for Mediterranean-type ecosystems. P_c increases in 64.9% of the pixels, in which 71.1% of the increase occurs in Eurasia and 3.5% of the increase is over 2 mm yr^{-1}. P_c decreases occur mainly in North America, albeit heterogeneously, e.g., the southwest of Canada and the eastern coastal United States (Figure 4d).

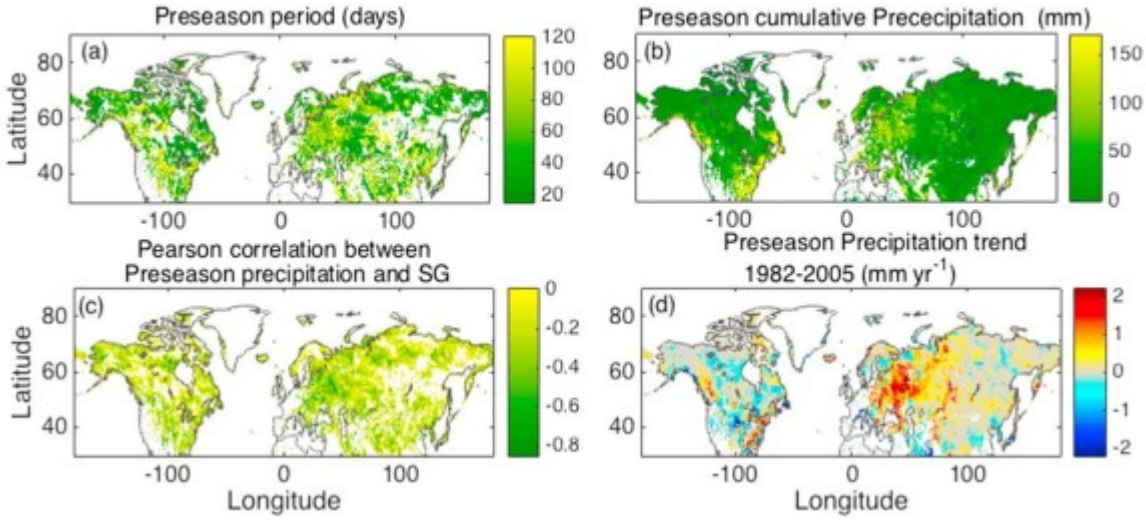

Figure 4

CRU-NCEP preseason cumulative precipitation corresponding to GIMMS SG: (a) the duration of the preseason period of precipitation control (P_P), (b) the cumulative precipitation in P_P (P_c), (c) the PCC between P_c and SG, and (d) the P_c trend over 1982–2005.

3.3 Simulated Preseason Correlations With the SG

In addition to the observations, we analyzed the preseason climate (T_m and P_c) for the five ESMs that made available daily temperature and precipitation outputs. ESMs show diverse performance in predicting the dependence of the SG on T_m (Figure 5). Except for CCSM4, the ESMs we analyzed tend to predict lower correlations between T_m and SG, as compared to CRU-NCEP (Figures 3c and 3d). CCSM4 and IPSL-CM5A resemble the observed spatial dependence of SG on T_m between 45 and 70°N (Figures 5a and 5g). However, CCSM4 estimated stronger SG dependence on T_m with PCC above 0.5 in 81.5% of the pixels and a warming P_T predicted in 90.2% of the valid CCSM4 pixels (Figures 5d, 5f, 5h, and 5j). The other four models also predicted dominant warming during P_T, although the areal extent of warming P_T is much reduced with strong spatial heterogeneity. Between 30 and 80°N, the predicted zonal mean warming of 0.73 ± 0.15°C per decade agrees quite well with CRU-NCEP based warming of 0.75 ± 0.16°C per decade. CRU-NCEP-based cooling in west of the Baltic Sea is partly reproduced by INM-CM4 (Figure 5f) and MPI-ESM-LR (Figure 5j). The positive bias in the zonal-mean warming over 53–61°N and 73–77°N is mainly attributed to the predicted stronger warming in the North America (Figure 5k).

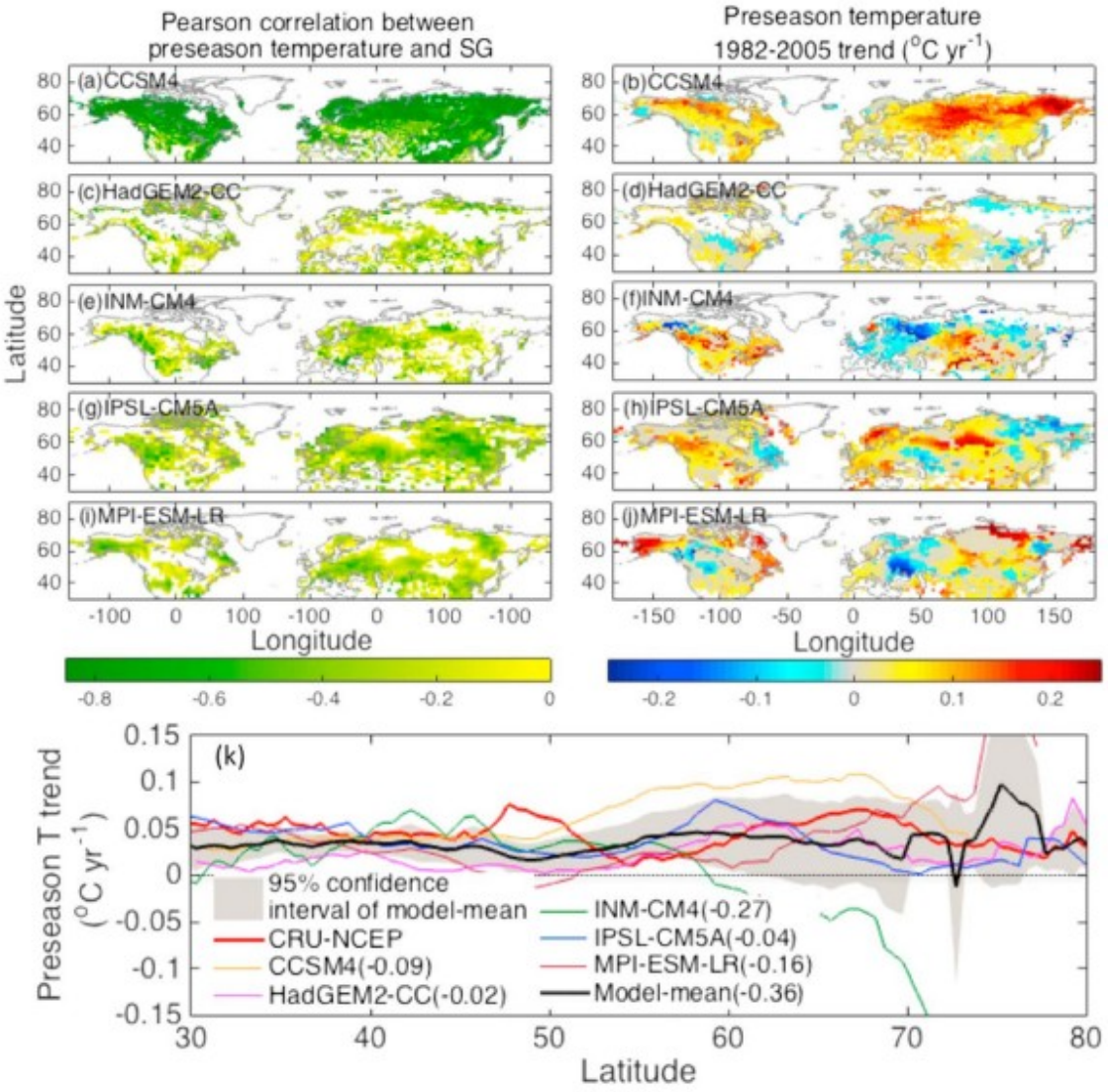

Figure 5

Correlations within ESMs (a, c, e, g, and i) between preseason temperature and spring greenup (SG), (b, d, f, h, and j) the trend of preseason temperature in each ESM, and (k) the zonal mean trend of preseason temperature trends across ESMs and observations. The numbers in legend indicate the correlation between model and CRU-NCEP preseason temperature trend.

The ESMs that we analyzed tend to predict higher correlation between P_c and SG than CRU-NCEP (Figure 6; compare to Figures 4c and 4d). Only CCSM4 resembles CRU-NCEP in this regard, with a lower correlation between P_c and SG than that between T_m and SG (Figure 6a). The ESMs, other than MPI-ESM-LR, reproduced the observed strong precipitation dependence of SG in the northeast of the Mediterranean Sea where wetting P_P is predicted in agreement with the CRU-NCEP (Figures 6b, 6d, 6f, 6h, and 6g). In contrast to the CRU-NCEP, more areas are subject to drying P_P in Eurasia in all ESMs. The zonal mean P_c trend shows that CRU-NCEP-based P_c trend lies within the 95% confidence interval of the model mean, despite the scattered predictions (Figure 6k). According to the latitudinal drying-wetting transition, the

simulated wetting P_P over 33–37°N of 1.6 ± 1.1 mm per decade is consistent with the CRU-NCEP derived wetting trend of 1.5 ± 1.1 mm per decade. Both the observations and simulations show a drying P_P over 37–67°N, although the drying trend is larger in the simulations. No significant variation in P_c was observed or predicted in the north of 70°N.

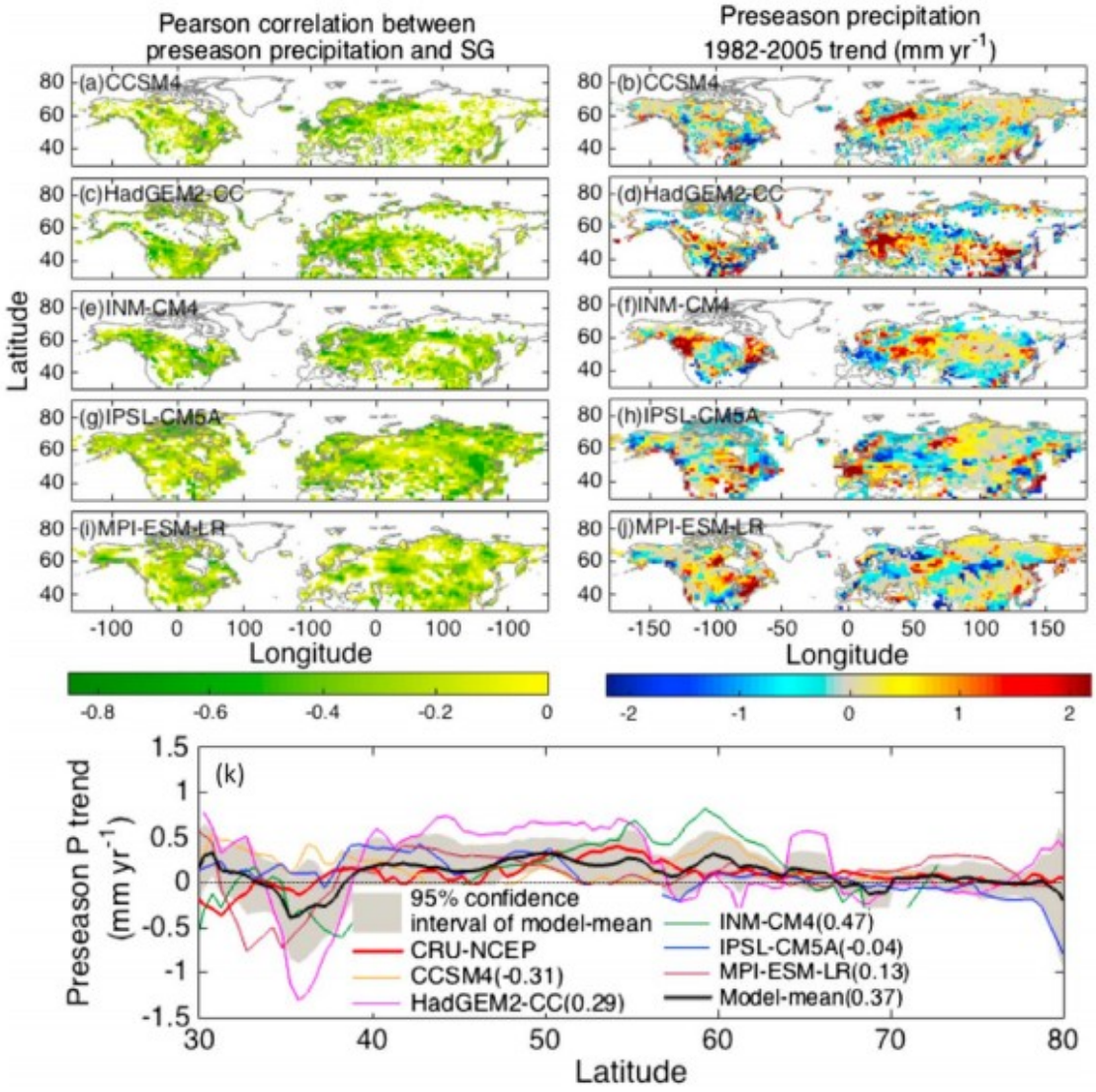

Figure 6

Simulated correlations (a, c, e, g, and i) between preseason precipitation and spring greenup (SG) in CMIP5 ESMs, (b, d, f, h, and j) the trend of preseason precipitation in ESMs, and (k) the zonal mean trend of preseason precipitation in observations and ESMs. The numbers in legend indicate the correlation between model and CRU-NCEP preseason precipitation trend.

The intermodel differences in the correlation between the preseason climate and SG, as well as the trends of the preseason climate, are also associated with the various ESM predictions of preseason period and preseason climate (Figures 7 and 8). Four ESMs (not CCSM4) tend to predict longer P_T than CRU-NCEP in some regions, e.g., eastern Asia by INM-CM4, western Europe, and

eastern U.S. by MPI-ESM-LR. CCSM4 and HadGEM2-CC significantly overestimate the T_m, while INM-CM4, IPSL-CM5A, and MPI-ESM-LR underestimate T_m in the north of 45°N (Figure 7). The predicted P_P is not prolonged compared to predicted P_T. All five ESMs tend to overestimate P_c over 40–60°N in both Eurasia and North America (Figure 8). Even though we analyzed the preseason period and climate across biomes, the biases are still significant for $P_T$and P_c (Figure 9). The overestimation of the P_T compared to that derived from CRU-NCEP ranges from 8 to 23 days across biomes. Despite the overestimation, the interbiome variability of P_T is captured by CCSM4, INMCM4, MPI-ESM-LR, and the multimodel mean ($r \geq = 0.79$, $p \leq 0.03$). INM-CM4, IPSL-CM5A, MPI-ESM-LR, and the multimodel mean captured the observed interbiome variability in T_m ($r \geq =0.85$, $p < 0.01$), while CCSM4 and HadGEM2-CC tend to estimate too high T_m ($r \geq 0.58$, $p \leq 0.07$). T_m ranges from 0.8 to 5°C for CCSM4 and from 4.5 to 21.8°C for HadGEM2-CC. Only CCSM4 reproduced the interbiome variability in P_P ($r = 0.8$, $p < 0.01$). All the ESMs predicted much higher P_c than CRU-NCEP with great variability among the ESMs. Despite the overestimate, CCSM4 captured the interbiome variability in P_c ($r = 0.85$, $p < 0.01$).

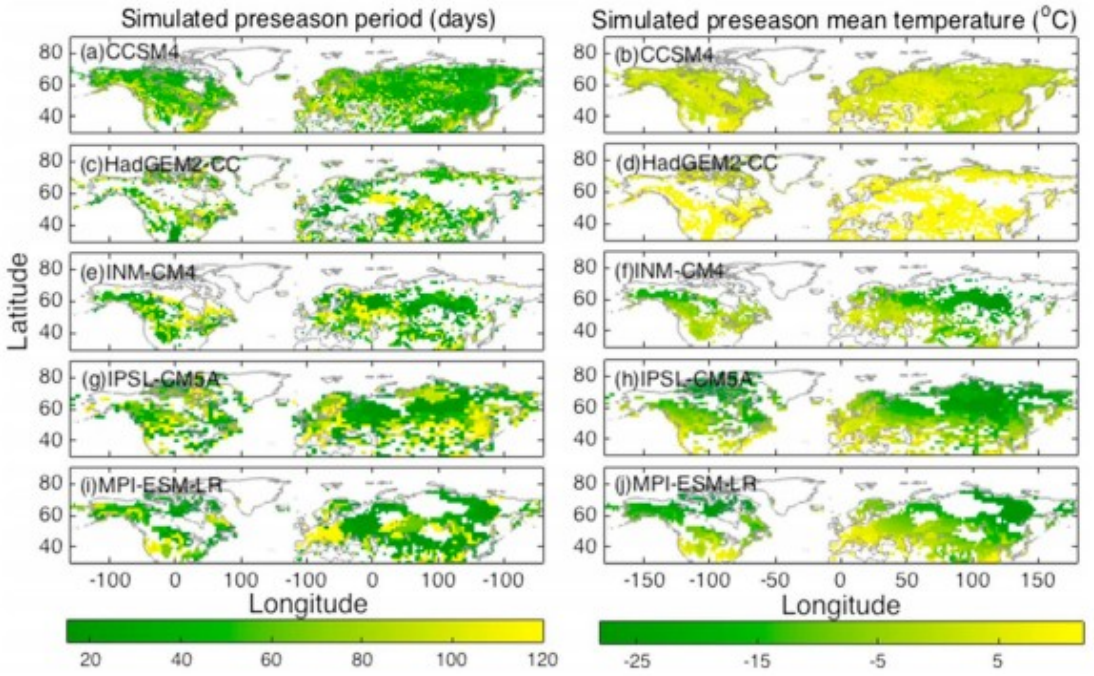

Figure 7

(a, c, e, g, and i) Duration of the preseason period of temperature control (P_T) in CMIP5 ESMs and (b, d, f, h, and j) the mean temperature during the P_T (T_m), as simulated by CMIP5 ESMs, over the period 1982–2005.

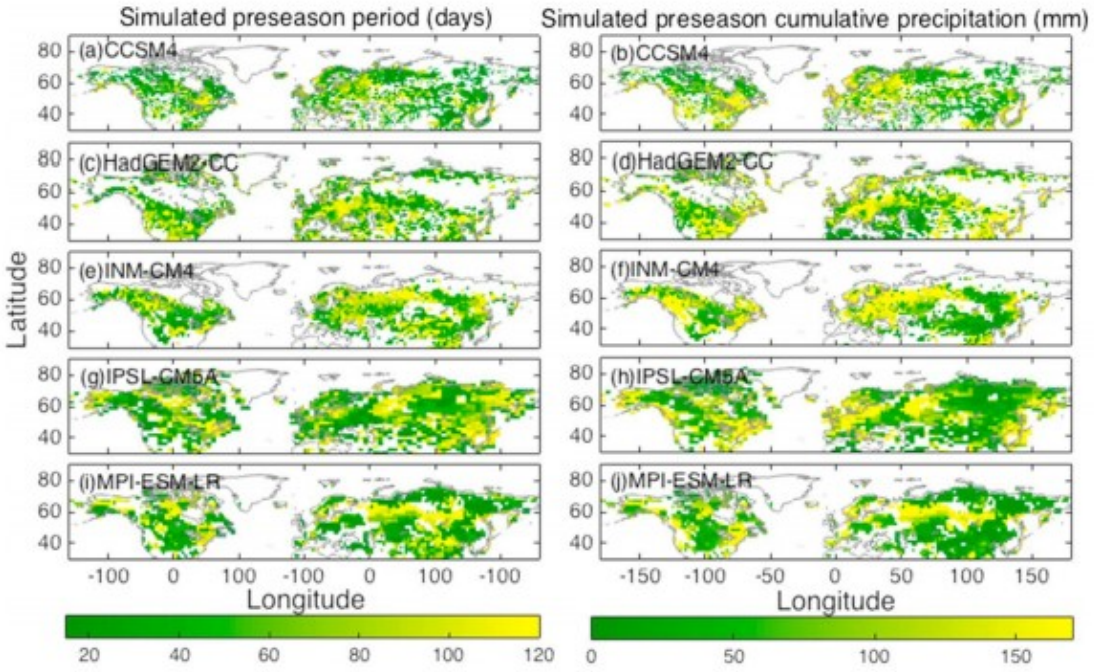

Figure 8

(a, c, e, g, and i) Duration of the preseason period of precipitation control (P_P) in CMIP5 ESMs and (b, d, f, h, and j) the mean precipitation during the P_P (P_c) as simulated by CMIP5 ESMs over the 1982–2005 period.

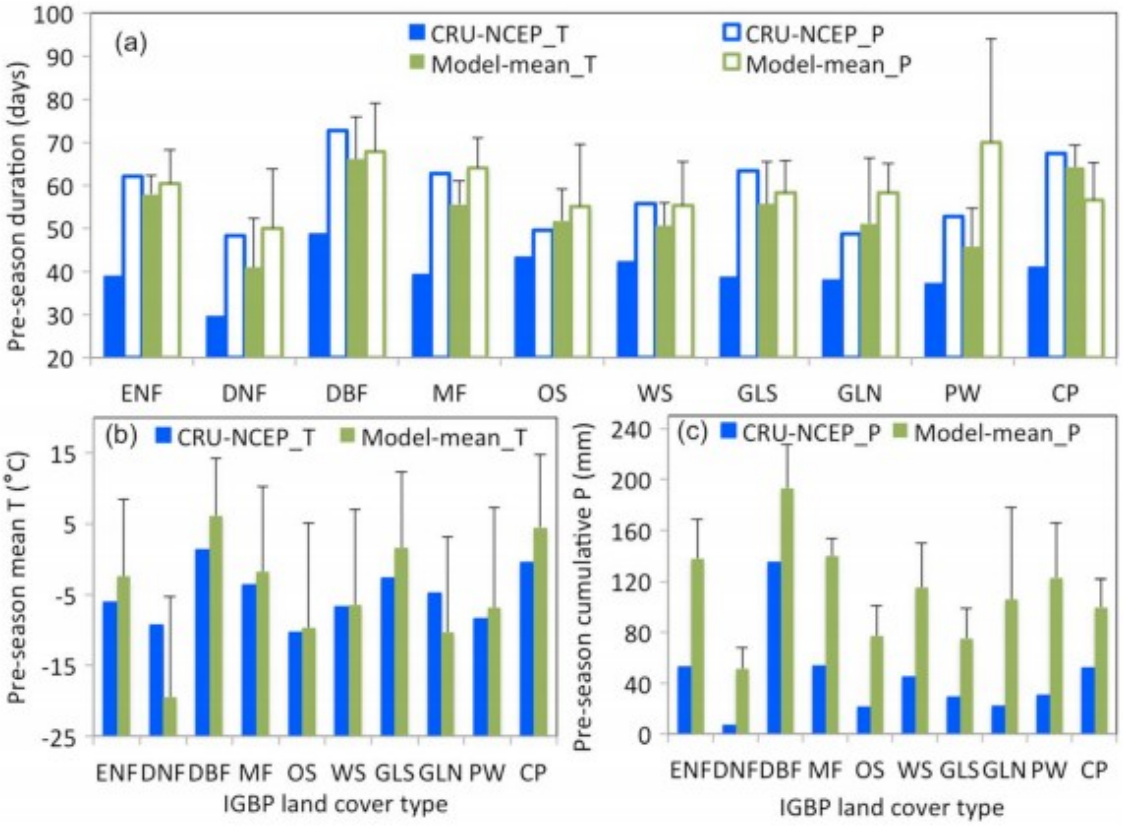

Figure 9

Preseason period, as observed and simulated by CMIP5 ESMs, for (a) temperature (CRU-NCEP_T and Model-mean_T) and precipitation (CRU-NCEP_P and Model-mean_P) control, and (b) the mean temperature and (c) cumulative precipitation during the respective periods. The error bars are the standard deviations of preseason period, T_m and P_c in individual models.

3.4 Spring Greenup in Response to Climate

The spatial heterogeneity of SG shifts is attributed to heterogeneous preseason climate changes and the different responses of plants to climate change. We calculated the response of the SG to preseason climate by calculating linear regressions between time series of SG and T_m (and P_c) over the studied years.

3.4.1 SG Sensitivities to Preseason Temperature

The T_m sensitivity of GIMMS-based SG shifts indicates that the SG is most sensitive to T_m in temperate and southern boreal regions (Figures 10a–10f). The dominant biomes in the temperate region are deciduous broadleaf forests in the southeast of the United States, mixed forests in the northeast of the United States and Central Eurasia, temperate grasslands in midwest of the United States and mid-South Asia, and croplands in the central of the United States and the east of Europe and China. The observed sensitivities of the SG to T_m across biomes are most significant in forests: deciduous broadleaf forests (−3.3 days per °C), mixed forests (−2.6 days per °C),

evergreen needleleaf forests (−2.4 days per °C), temperate grasslands (−2.2 days per °C), croplands (−2.0 days per °C), boreal woody savannas (−1.3 days per °C), open shrublands (−0.8 days per °C), and northern grasslands (−0.7 days per °C) (Figure 10g). The SG sensitivities to T_m in deciduous needleleaf forest are low compared with other temperate and boreal forests (−0.7 days per °C) (Figure 10g).

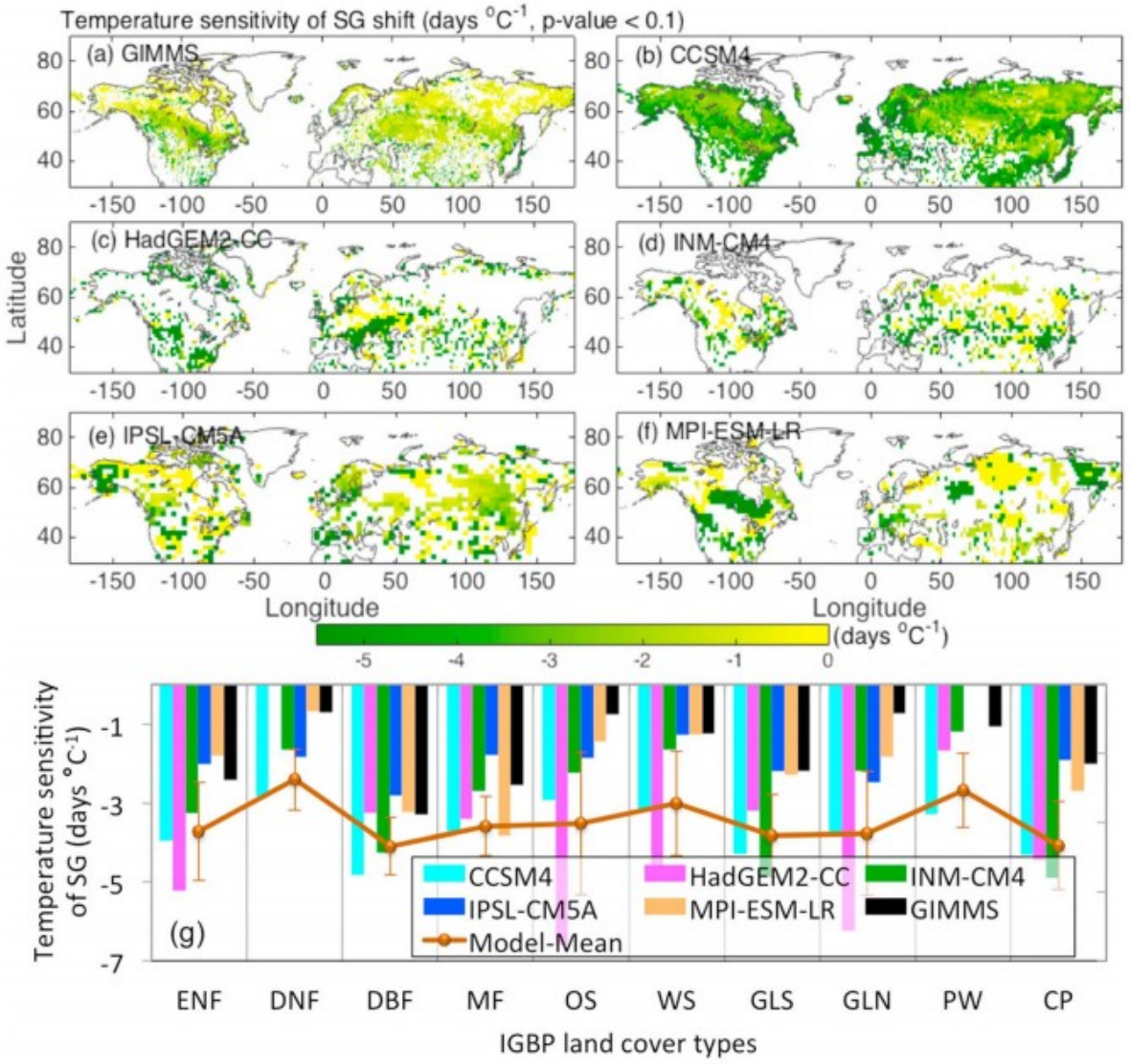

Figure 10

Temperature sensitivity of spring greenup (SG), as inferred from correlations over the period (1982–2005) in (a) GIMMS, (b–f) ESMs, and (g) across biomes. The numbers of pixels that were used to calculate the biome-scale temperature sensitivity of SG are shown in Table S3.

The ESMs demonstrated a T_m control on SG in the temperate and boreal regions, but none of the ESMs capture the magnitude and observed spatial pattern of the T_m control on SG (Figure 10). Across biomes, the modeled spatial transitions of T_m control on SG are not smoothly distributed, leading to some extreme dependence of SG on T_m. For example, $T_m$sensitivities of SG

for deciduous broadleaf forests by INM-CM4 and SG for open shrublands by HadGEM2-CC are as large as −8.5 days per °C (Figure 10g). CCSM4, INM-CM4, and MPI-ESM-LR tend to overestimate SG shifts in response to T_m. Even so, the T_m sensitivities of SG across biomes by CCSM4, INM-CM4, and MPI-ESM-LR are well spatially correlated to that by GIMMS ($r > 0.72$, $p < 0.01$) (Figure 11).

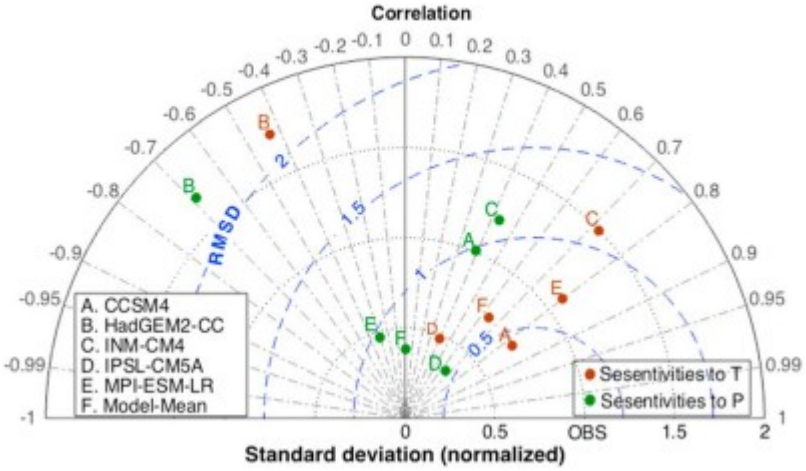

Figure 11

Taylor diagram showing inter-biome temperature and precipitation sensitivities for the five ESMs relative to that derived from GIMMS.

3.4.2 SG Sensitivities to Preseason Precipitation

The area in which the SG shift depends strongly on P_c is relatively smaller than for T_m in both GIMMS- and ESM-derived SG shifts (Figure 12). Only the region in the north of Mediterranean shows pronounced observed responses to P_c. P_c sensitivities of SG shift are −0.26 days $\%^{-1}$ (in precipitation increase) in deciduous broadleaf forests, followed by −0.18 days $\%^{-1}$ in evergreen needleleaf forests, −0.17 days $\%^{-1}$ in mixed forests, −0.15 days $\%^{-1}$ in croplands, and −0.13 days $\%^{-1}$ in temperate grasslands. The boreal biomes, woody savannas (−0.07 days $\%^{-1}$), deciduous needleleaf forest (−0.05 days $\%^{-1}$), open shrublands (−0.04 days $\%^{-1}$), and northern grasslands (−0.03 days $\%^{-1}$) show weak response to P_c (Figure 12g).

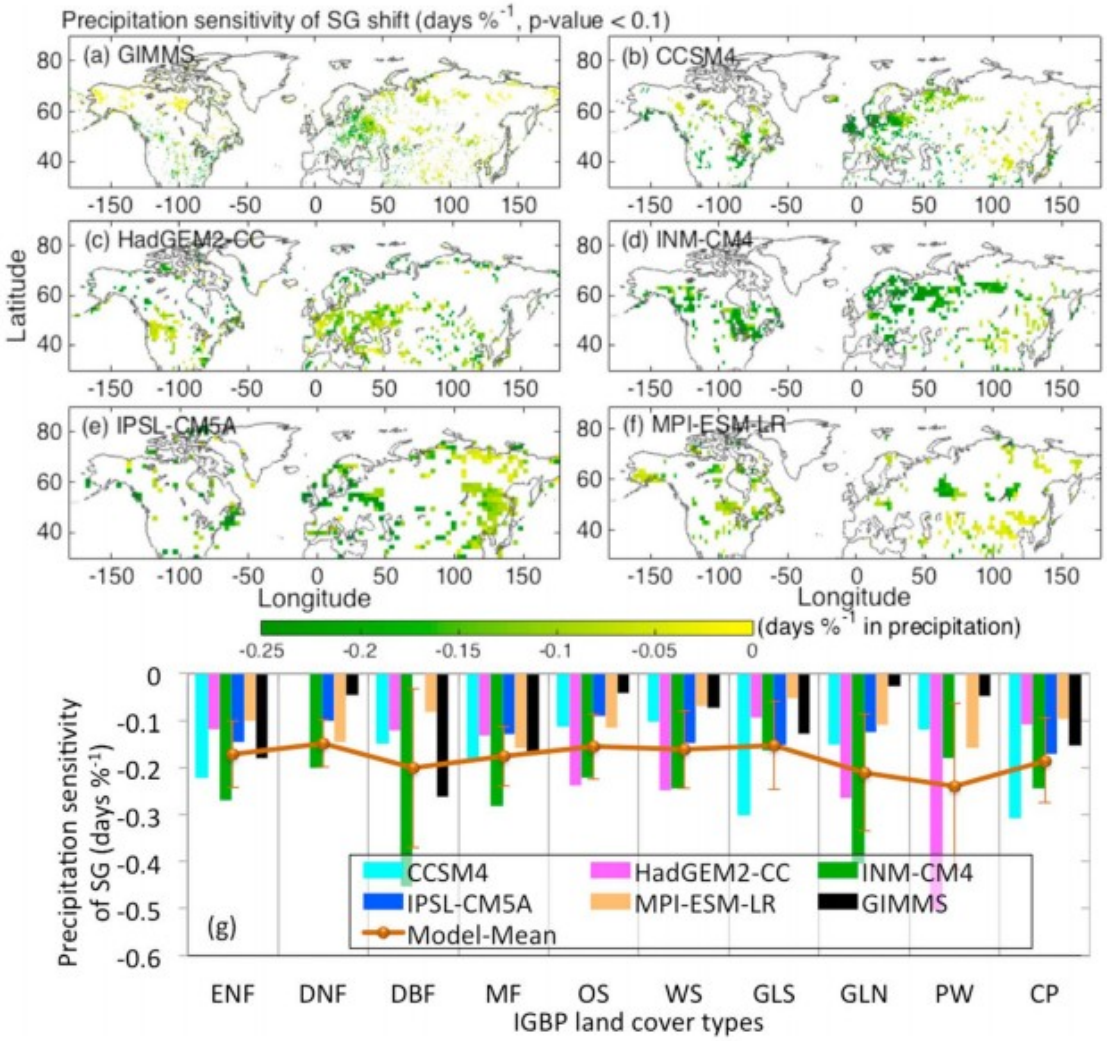

Figure 12

Precipitation sensitivity of spring greenup (SG), as inferred from correlations over the period (1982–2005) in (a) GIMMS, (b–f) ESMs, and (g) across biomes. The numbers of pixels that were used to calculate the biome-scale precipitation sensitivity of SG are shown in Table S3.

CCSM4, HadGEM2-CC, INM-CM4, and IPSL-CM5A predicted part of the pronounced $P_c$sensitivities of SG shift in the north of Mediterranean (Figures 12b–12e). The modeled mean biome P_c sensitivities are approximately equal to that derived by GIMMS (−0.20 days $\%^{-1}$ in deciduous broadleaf forests, −0.17 days $\%^{-1}$ in evergreen needleleaf forests, −0.18 days $\%^{-1}$ in mixed forests, −0.18 days $\%^{-1}$ in croplands, and −0.15 days $\%^{-1}$ in temperate grasslands). However, P_c sensitivities are significantly overestimated in the northern biomes (−0.16 days $\%^{-1}$ in woody savannas, −0.15 days $\%^{-1}$ in deciduous needleleaf forest, −0.16 days $\%^{-1}$ in open shrublands, and −0.24 days $\%^{-1}$ in northern grasslands). Despite the overestimates, interbiome P_c sensitivities by IPSL-CM5A are better correlated to GIMMS ($r = 0.65$, $p < 0.10$) than the other models (Figure 11).

4 Discussion

4.1 Preseason Climate

The preseason climate change differs from annual and seasonal climate changes. The northern hemisphere spring (March, April, and May) warming is enhanced over the 1979–2005 period relative to the northern hemisphere annual warming over that period (Solomon et al., 2007). The warming in CRU-NCEP derived P_T over 1982–2005 (0.75 °C per decade) is almost double the spring warming of 0.39 °C per decade over 1988–2010 (Cohen et al., 2012). The spatial pattern of P_c agrees with the annual precipitation trend over 1979–2005 (Solomon et al., 2007): slight drying trend over North American and strong wetting trend over Eurasia. This continental asymmetrical pattern results in a growing P_c trend of 0.84 ± 1.37 mm per decade in the Northern Hemisphere. The latitudinal trend suggests that the P_P in arid and humid areas is becoming drier and wetter, respectively. The P_c trend was insignificant relative to the other seasonal and annual precipitation trends (de Martino et al., 2013; Small et al., 2006). If annual, or even spring, climate is used as a proxy, the sensitivities of phenology change can be biased. We found that vegetation tends to respond to the climate just prior to SG rather than the climate through the whole spring season. A typical example is the delayed leaf emergence in the warmer spring of 2012 compared to the colder spring of 2010 in northeastern temperature forests of the U.S., where positive temperature anomalies occurred immediately prior to the leaf emergence in 2010 rather than anomalies in the early spring of 2012 (Friedl et al., 2014).

Phenology predictions rely on the very different climate driver predictions across the ESMs. The mean of the five participating ESMs showed a pattern of latitudinal warming of P_T in the northern hemisphere, a wetting of P_P between 37 and 67°N, and a drying of P_P around 35°N over 1982–2005; this mean model behavior agrees with the CRU-NCEP deviations. However, the spread across the ESM predictions and the spatial heterogeneity of the preseason climate trends are concealed in the model mean and zonal mean trends. These discrepancies are partially due to the internal dynamics of each model, and the relatively short period of comparison to the observations.

In comparison with CRU-NCEP, ESMs generally predict much longer P_T and slightly longer P_P. The model mean of T_m across biomes is moderately close to the observations. All the ESMs overestimate P_c. ESMs also overestimated annual precipitation, which caused systematic overestimation of evapotranspiration (Mueller & Seneviratne, 2014). These biases in precipitation and evapotranspiration influence soil moisture predictions (Yuan & Quiring, 2017), which are usually applied to spring phenology of PFTs with seasonal water stress (Text S1). The discrepancies in preseason climate and its spatial and temporal trends indicate that constraints on spatial and temporal variations of preseason climate are weak. Further, these discrepancies can strongly affect climate mediated ecological processes, such as spring phenology.

We derived the preseason climate from ESM-predicted coupled climate-vegetation dynamics. The reported overestimation of ESM-predicted LAI attributed to wet biases (Anav et al., 2013) and growing season lengths (Murray-Tortarolo et al., 2013) can lead to biases in determining the simulated SG and thus its correlated preseason period and climate. Another source of uncertainty in the ESM-derived SG and preseason climate results from differences in ESM PFT classifications, which can affect LAI, and thus determination of phenological thresholds. For instance, in the land component of the ESMs, there are 15 PFTs in CCSM4 CLM4, 12 PFTs in MPI-ESM JSBACH and IPSL-CM5A ORCHIDEE, and 5 PTFs in HadGEM2-CC JULES (Poulter et al., 2015). The spatial distribution and represented vegetation dynamics of the PFTs are different in ESMs (Sitch et al., 2008).

4.2 SG Sensitivities to Climate

The GIMMS-derived SG indicates an advancing SG in the Northern Hemisphere over 1982–2005, despite considerable variability across biomes and regions. Deciduous broadleaf forests and mixed forests show the greatest SG advances (3.1 and 1.9 days per decade), in response to T_m increases of −3.3 and −2.6 days per °C, and P_c increases of −0.26 and −0.17 days $\%^{-1}$, respectively. The CMIP5 ESM SG advances in temperate forests are in the range of previously modeled and other satellite-based results (Jeong et al., 2011; Richardson et al., 2006; Vitasse et al., 2009), although interdecadal variations in SG advances (Delbart et al., 2008; Jeong et al., 2011) are potentially ignored in the general trend in our analysis over 1982–2005. Although the SG of evergreen needleleaf forests strongly relies on the T_m and P_c, the advances are much smaller than deciduous broadleaf and mixed forests. For the temperate and boreal woody species, it is widely recognized that besides accumulated temperature, chilling requirements and photoperiod are essential for bud development and that these requirements differ among species (Polgar & Primack, 2011). Among forest biomes, the T_m and P_c sensitivities of SG shifts are low in deciduous needleleaf forests; thus, there is only a small SG advance over 1982–2005.

Our cropland SG estimates (from GIMMS) indicate an advance of 1.15 days per decade over 1982–2005 in response to preseason warming (−2.03 days per °C). The SG advancing trend in croplands is similar to the recorded trends in agricultural and horticultural events over 1951–2004 in Germany (Estrella et al., 2007) and wheat heading trends over 1948–2004 in the U.S. Great Plains (Hu et al., 2005), although the SG sensitivity is less than the recorded rate of −3.7 days per °C to spring temperature (Estrella et al., 2007). Adjusted sowing dates were reported to accommodate the warming climate. For example, potato sowing dates advanced by about 5 days over 1965–1999 in Finland (Hildén et al., 2005); sowing dates advanced up to 1 month over the past 30 years ago for maize and winter wheat in France (Menzel, von Vopelius, et al., 2006); in the US, corn planting dates advanced about 10 days from 1981 to 2005, and soybean planting dates advanced about 12 days (Sacks & Kucharik, 2011). Our results indicate that the SG of

crops strongly correlates with P_c (−0.15 days $\%^{-1}$), which may be applicable to nonirrigated crops. Although many studies have revealed the influence of water availability on crop growth and yield, the precipitation dependency of crop SG is rarely discussed, possibly due to the fact that water supply of croplands is often affected by irrigation (Li et al., 2004; Zhang & Oweis, 1999) and crop management practice. Under water-limited conditions, crops with enhanced drought stress tolerance can replace less stress-tolerant species (Farooq et al., 2009; Valliyodan & Nguyen, 2006).

Biomes in the north (open shrublands, woody savannas, and northern grasslands) show relatively low SG sensitivities to T_m and P_c. In IGBP vegetation classifications, large areas of open shrublands are located in the northern high latitude. According to IGBP classification, open shrubland in the northern part of North America and Russia tundra zones are overestimated and can be better classified as grasslands (Friedl et al., 2010). These northern ecosystems more closely follow the preseason climate sensitivities of northern grasslands. The International Tundra Experiment control data showed low SG advance in tundra in response to background temperature (Oberbauer et al., 2013). The low sensitivities of SG to T_m and P_c are probably due to the timing of snowmelt, which also affects high Arctic spring phenology (Hoye et al., 2007). The effects of altered snowmelt patterns can even reverse the effects of warmer temperature on phenological processes (Bjorkman et al., 2015). A warmer winter may also result in chilling requirements not being met, and thus affect spring phenology (Yu et al., 2010), which could counter the spring warming-caused SG advance.

Over 1982–2005, GIMMS-derived southern grassland SG advanced at 0.87 days per decade in response to T_m at the rate of −2.20 days per °C and P_c at the rate of −0.13 days $\%^{-1}$. These advancement rates are comparable to the observed SG advance of 0.95 days per decade in China (Ma & Zhou, 2012) but much smaller than the recorded bloom advance of grassland species in the Rocky Mountains (−6.1 days per decade) (Lesica & Kittelson, 2010). In arid and semiarid systems, influences of water availability on vegetation growth obtained much concern due to water-limited conditions. Water stress effects are related to both drought intensity and length (Vicente-Serrano et al., 2013) and precipitation patterns of frequency and seasonal distribution (Miranda et al., 2011). Multiple studies indicate that SG in arid and semiarid regions is driven by both temperature and water (Moore et al., 2015; Shen et al., 2011), although temperature may still be the predominant driver (Seghieri et al., 2012).

The five ESMs each predicted varied SG advance rates and T_m sensitivities. The ESM-predicted T_m sensitivities across biomes are usually overestimated relative to GIMMS. INM-CM4 and IPSL-CM5A best represented GIMMS-derived P_c sensitivities of SG across biomes. We find that the correlation between the CCSM4 modeled T_m sensitivities for five forest biomes is highly correlated to that by GIMMS ($r = 0.95$, $p < 0.01$). The correlation between the CCSM4

modeled P_c sensitivities of its SG and that by GIMMS increased from 0.39 for all biomes to 0.89 for nonforest biomes. Furthermore, improved LAI prediction by ESMs with more PFTs has been reported (Murray-Tortarolo et al., 2013), which may improve predictions of LAI phenology.

4.3 Uncertainties in ESM Evaluation

In this study, we used preseason temperature and precipitation as SG precursors. The effects of other cues, such as accumulative chilling, snow cover, and photoperiod, may also play important roles in regulating the SG but are not typically included in ESMs. Monthly average daily maximum temperatures were found to be more important than minimum and mean temperatures in controlling interannual SG variation in Europe and the United States (Piao et al., 2015). In contrast, the minimum daily preseason temperature plays a more important role in determining SG than minimum daily preseason temperature over Tibetan Plateau (Shen et al., 2016). Observational studies that specifically analyze plant phenological controls amenable to ESM land model integration are required across regions, biomes, and topographies.

We used the GIMMS NDVI3g-inferred SG to evaluate the simulated LAI inferred SG. GIMMS NDVI3g is widely used for its long time span that has the longest overlapping period with ESMs historical simulations (1982–2005). However, in this period, GIMMS NDVI3g has been criticized for potential quality issues. GIMMS NDVI-inferred SG is different from SPOT NDVI and MODIS EVI inferred SG in Tibetan Plateau (Shen, Zhang, et al., 2014) and Arctic (Zeng, Jia, & Forbes, 2013) after 2001, which was attributed to quality issue in GIMMS NDVI, especially in most parts of the western Tibetan Plateau (Zhang et al., 2013). To better assess vegetation dynamics, multiple data sets were suggested for inter-validation (Brown et al., 2006; Shen, Zhang, et al., 2014). For our analysis of SG sensitivities to climate variables, we skipped the pixels in which climate-SG correlations are insignificant ($p \geq 0.1$), which can potentially screen out the NDVI-derived SG that are not driven by temperature and precipitation forcing.

5 Concluding Remarks

We analyzed the spring phenology and its responses to climate change in north temperate and boreal regions (>30°N) with GIMMS NDVI and ESMs modeled LAI over 1982–2005. We first analyzed the preseason dynamics, defined as the period preceding spring greenup during which the mean temperature (T_m) and cumulative precipitation (P_t) regulate the timing of SG. T_m warmed ~0.75 °C decade^{-1} over 1982–2005, a value higher than warming that occurred over spring and annually. The wetting preseason occurred in relatively humid areas and drying preseason in relatively dry areas. We next analyzed the phenological responses: GIMMS NDVI-derived SG shows advances of about 1 day per decade in the northern midlatitudes with significant spatial heterogeneity. The spatial heterogeneity of SG results

from heterogeneous climate change during the preseason and various responses to preseason climate across regions and vegetation biomes.

Although the extent of the regions with preseason precipitation dependency is smaller than that for temperature, the biomes that are more sensitive to temperature are also more sensitive to precipitation, suggesting an interactive control of temperature and precipitation. The GIMMS-based SG in response to preseason climate across biomes is subject to the shortcoming that the effects of cues, such as accumulative chilling, snow cover, and photoperiod, are ignored in our analysis. Most ESMs, especially the ESM multimodel mean, were able to represent observationally inferred latitudinal preseason climate and SG trends. However, the spatial pattern, and periods and climate of preseason across biomes were not well represented. In particular, wet biases in P_c are present in all five of the ESMs that we analyzed. This wet bias may have affected LAI predictions, thus further biasing predicted SG. The discrepancies between modeled and observed climate controls on SG reveal the uncertainties in predicting terrestrial phenology and carbon cycles, including those associated with climate forcing and land-atmosphere interactions.

Phenology is a critical driver of coupled land-atmosphere exchanges and C cycling and is expected to change in response to changing climate. Although the ESM multimodel mean roughly matches observationally derived trends in SG and preseason climate, no individual ESM accurately predicted these trends or controls. Reducing these biases should start from reducing biases in climate prediction. Further, understanding of the physics that govern the phenological processes and how these processes can be represented in regional-to-global-scale Earth system modeling should be further investigated.

Data

The CMIP5 data were downloaded through https://esgf-node.llnl.gov/projects/esgf-llnl/. MODIS IGBP land cover type classification is obtained from http://glcf.umd.edu/data/lc/. GIMMS NDVI3g is available from https://nex.nasa.gov/nex/projects/1349/. The introduction to CRU-NCEP V6 is available from http://forge.ipsl.jussieu.fr/orchidee/wiki/Documentation/Forcings.

Acknowledgments

This study is funded by National Natural Science Foundation of China (NSFC) (41590853) and grant from CAS Pioneer Hundred Talents Program. We acknowledge support from the U.S. Department of Energy, Office of Science, Biological and Environmental Research, Regional and Global Climate Modeling Program through the RUBISCO Scientific Focus Area under contract DE-AC02-05CH11231 to Lawrence Berkeley National Laboratory. We acknowledge the World Climate Research Programme's Working Group on Coupled Modeling, which is responsible for CMIP, and we thank the climate

modeling groups for producing and making available their model outputs. For CMIP, the U.S. Department of Energy's Program for Climate Model Diagnosis and Intercomparison provides coordinating support and led development of software infrastructure in partnership with the Global Organization for Earth System Science Portals.

References

Ahas, R., Aasa, A., Menzel, A., Fedotova, V. G., & Scheifinger, H. (2002). Changes in European spring phenology. *International Journal of Climatology*, 22, 1727– 1738. https://doi.org/10.1002/joc.818

Anav, A., Murray-Tortarolo, G., Friedlingstein, P., Stich, S., Piao, S., & Zhu, Z. (2013). Evaluation of land surface models in reproducing satellite derived leaf area index over the high latitude-Northern Hemisphere. Part II: Earth system models. *Remote Sensing*, 5, 3637– 3661. https://doi.org/10.3390/rs5083637

Arora, V. K., & Boer, G. J. (2005). A parameterization of leaf phenology for the terrestrial ecosystem component of climate models. *Global Change Biology*, 11, 39– 59. https://doi.org/10.1111/j.1365-2486.2004.00890.x

Bjorkman, A. D., Elmendorf, S. C., Beamish, A. L., Vellend, M., & Henry, G. H. R. (2015). Contrasting effects of warming and increased snowfall on Arctic tundra plant phenology over the past two decades. *Global Change Biology*, 21, 4651– 4661. https://doi.org/10.1111/gcb.13051

Borner, A. P., Kielland, K., & Walker, M. D. (2008). Effects of simulated climate change on plant phenology and nitrogen mineralization in Alaskan arctic tundra. *Arctic, Antarctic, Alpine Research*, 40, 27– 38. https://doi.org/10.1657/1523-0430(06-099)%5BBORNER%5D2.0.CO;2

Böttcher, K., Markkanen, T., Thum, T., Aalto, T., Aurela, M., Reick, C. H., … Pulliainen, J. (2016). Evaluating biosphere model estimates of the starts of the vegetation active season in boreal forests by satellite observations. *Remote Sensing*, 8, 580. https://doi.org/10.3390/rs8070580

Brown, M. E., Pinzón, J. E., Didan, K., Morisette, J. T., & Tucker, C. J. (2006). Evaluation of the consistency of long-term NDVI time series derived from AVHRR, SPT-Vegetation, SeaWiFS, MODIS, and LandSAT ETM + Sensors. *IEEE Transactions on Geoscience and Remote Sensing*, 44, 1787– 1793. https://doi.org/10.1109/TGRS.2005.860205

Busetto, L., Colombo, R., Migliavacca, M., Cremonese, E., Meroni, M., Galvagno, M., … Pari, E. (2010). Remote sensing of larch phenological cycle and analysis of relationships with climate in the Alpine region. *Global Change Biology*, 16, 2504– 2517. https://doi.org/10.1111/j.1365-2486.2010.02189.x

Cannell, M. G. R., & Smith, R. I. (1983). Thermal time, chill days and prediction of budburst in *Picea sitchensis*. *Journal of Applied Ecology*, 20, 951– 963. https://doi.org/10.2307/2403139

Channan, S., Collins, K., & Emanuel, W. R. (2014). *Global Mosaics of the Standard MODIS Land Cover Type Data*. College Park, MD: University of Maryland and the Pacific Northwest National Laboratory.

Chen, X., Hu, B., & Yu, R. (2005). Spatial and temporal variation of phonological growing season and climate change impacts in temperate eastern China. *Global Change Biology*, 11, 1118– 1130. https://doi.org/10.1111/j.1365-2486.2005.00974.x

Cohen, J. L., Furtado, J. C., Barlow, M., Alexeev, V. A., & Cherry, J. E. (2012). Asymmetric seasonal temperature trends. *Geophysical Research Letters*, 39, L04705. https://doi.org/10.1029/2011GL050582

Cong, N., Wang, T., Nan, H., Ma, Y., Wang, X., Myneni, R. B., & Piao, S. (2013). Changes in satellite-derived spring vegetation green-up date and its linkage to climate in China from 1982 to 2010: A multimethod analysis. *Global Change Biology*, 19, 881– 891. https://doi.org/10.1111/gcb.12077

De Beurs, K. M., & Henebry, G. M. (2005). Land surface phenology and temperature variation in the international geosphere-biosphere program high-latitude transects. *Global Change Biology*, 11, 779– 790. https://doi.org/10.1111/j.1365-2486.2005.00949.x

de Martino, G., Fontana, N., Marini, G., Singh, V. P., & Asce, F. (2013). Variability and trend in seasonal precipitation in the continental United State. *Journal of Hydrologic Engineering*, 18, 630– 640. https://doi.org/10.1061/(ASCE)HE.1943-5584.0000677

Delbart, N., Picard, G., Toan, T. L., Kergoat, L., Quegan, S., Woodward, I., ... Fedotova, V. (2008). Spring phenology in boreal Eurasia over a nearly century time scale. *Global Change Biology*, 14, 603– 614. https://doi.org/10.1111/j.1365-2486.2007.01505.x

Estrella, N., Sparks, T. H., & Menzel, A. (2007). Trends and temperature response in the phenology of crops in Germany. *Global Change Biology*, 13, 1737– 1747. https://doi.org/10.1111/j.1365-2486.2007.01374.x

Fan, L., Gao, Y., Brück, H., & Bernhofer, C. (2009). Investigating the relationship between NDVI and LAI in semiarid grassland in Inner Mongolia using in-situ measurements. *Theoretical and Applied Climatology*, 95, 151–156. https://doi.org/10.1007/s00704-007-0369-2

Farooq, M., Wahid, A., Kobayashi, N., Fujita, D., & Basra, S. M. A. (2009). Plant drought stress: effects, mechanisms and management. *Agronomy for Sustainable Development*, 29, 185– 212. https://doi.org/10.1051/agro:2008021

Friedl, M. A., Gray, J. M., Melaas, E. K., Richardson, A. D., Hufkens, K., Keenan, T. F., ... O'Keefe, J. (2014). A tale of two springs: using recent climate anomalies to characterize the sensitivity of temperate forest phenology to climate change. *Environmental Research Letters*, 9(5), 054006. https://doi.org/10.1088/1748-9326/9/5/054006

Friedl, M.A., Sulla-Menashe, D., Tan, B., Schneider, A., Ramankutty, N., Sibley, A., & Huang, X. (2010). MODIS Collection 5 global land cover: Algorithm refinements and characterization of new datasets, 2001–2012, Collection 5.1 IGBP Land Cover, Boston University, Boston, MA.

Gordo, O., & Sanz, J. J. (2010). Impact of climate change on plant phenology in Mediterranean ecosystems. *Global Change Biology*, 16, 1082– 1106. https://doi.org/10.1111/j.1365-2486.2009.02084.x

Green, E. P., Mumby, P. J., Edwards, A. J., Clark, C. D., & Ellis, A. C. (1997). Estimating leaf area index of mangroves from satellite data. *Aquatic Botany*, 58, 11– 19. https://doi.org/10.1016/S0304-3770(97)00013-2

Hänninen, H. (1990). Modeling bud dormancy release in trees from cool and temperate regions. *Acta Forestalia Fennica*, 213, 1– 47.

Hildén, M., Lehtonen, H., Bärlund, I., Hakala, K., Kaukoranta, T., & Tattari, S. (2005). The practice and process of adaptation in Finnish agriculture. 5, −34, Helsinki, Finnish Environment Institute Mimeographs 335. FINADAPT Working paper 5.

Hoye, T. T., Post, E., Meltofte, H., Schmidt, N. M., & Forchhammer, M. C. (2007). Rapid advancement of spring in the high Arctic. *Current Biology*, 17, R449– R451. https://doi.org/10.1016/j.cub.2007.04.047

Hu, Q., Weiss, A., Feng, S., & Baenziger, P. S. (2005). Earlier winter wheat heading dates and warmer spring in the U.S. Great Plains. *Agricultural and Forest Meteorology*, 135, 284– 290. https://doi.org/10.1016/j.agrformet.2006.01.001

Inouye, D. W. (2008). Effects of climate change on phenology, frost damage, and floral abundance of montane wildflowers. *Ecology*, 89, 353– 362. https://doi.org/10.1890/06-2128.1

Jeong, S.-J., Ho, C.-H., Gim, H.-J., & Brown, M. E. (2011). Phenlogy shifts at start vs. end of growing season in temperate vegetation over the Northern Hemisphere for the period 1982–2008. *Global Change Biology*, 17, 2385–2399. https://doi.org/10.1111/j.1365-2486.2011.02397.x

Jeong, S. J., Ho, C. H., & Jeong, J. H. (2009). Increase in vegetation greenness and decrease in springtime warming over East Asia. *Geophysical Research Letters*, 36, L02710. https://doi.org/10.1029/2008GL036583

Ji, J. (1995). A climate-vegetation interaction model: simulating physical and biological processes at the surface. *Journal of Biogeography*, 22, 445– 451. https://doi.org/10.2307/2845941

Kikuzawa, K. (1995). Leaf phenology as an optimal strategy for carbon gain in plants. *Canadian Journal of Botany*, 73, 158– 163. https://doi.org/10.1139/b95-019

Kramer, K. (1994). Selecting a model to predict the onset of growth of *Fagus sylvatica*. *Journal of Applied Ecology*, 31, 172– 181. https://doi.org/10.2307/2404609

Krinner, G., Viovy, N., de Noblet-Ducoudré, N., Ogée, J., Polcher, J., Friedlingstein, P., … Prentice, I. C. (2005). A dynamic global vegetation model for studies of the coupled atmosphere-biosphere system. *Global Biogeochemical Cycles*, 19, GB1015. https://doi.org/10.1029/2003GB002199

Lesica, P., & Kittelson, P. M. (2010). Precipitation and temperature are associated with advanced flowering phenology in a semi-arid grassland. *Journal of Arid Environments*, 74, 1013– 1017. https://doi.org/10.1016/j.jaridenv.2010.02.002

Li, F., Wang, P., Wang, J., & Xu, J. (2004). Effects of irrigation before sowing and plastic film mulching on yield and water uptake of spring wheat in semiarid Loess Plateau of China. *Agricultural Water Management*, 67, 77– 88. https://doi.org/10.1016/j.agwat.2004.02.001

Ma, T., & Zhou, C. (2012). Climate-associated changes in spring plant phenology in China. *International Journal of Biometeorology*, 56(2), 269– 275. https://doi.org/10.1007/s00484-011-0428-3

Menzel, A., Sparks, T. H., Estrella, N., Koch, E., Aasa, A., Ahas, R., … Zust, A. (2006). European phonological response to climate change matches the warming pattern. *Global Change Biology*, 12, 1969– 1976. https://doi.org/10.1111/j.1365-2486.2006.01193.x

Menzel, A., von Vopelius, J., Estrella, N., Schleip, C., & Dose, V. (2006). Farmers' annual activities are not tracking the speed of climate change. *Climate Research*, 32, 201– 207.

Miller-Rushing, A. J., & Primack, R. B. (2008). Global warming and flowering times in Thoreau's concord: a community perspective. *Ecology*, 89, 332– 341. https://doi.org/10.1890/07-0068.1

Miranda, J. D., Armas, C., Padilla, F. M., & Pugnaire, F. I. (2011). Climatic change and rainfall patterns: effects on semi-arid plant communities of the Iberian Southeast. *Journal of Arid Environments*, 75, 1302– 1309. https://doi.org/10.1016/j.jaridenv.2011.04.022

Moore, L. M., Lauenroth, W. K., Bell, D. M., & Schlaepfer, D. R. (2015). Soil water and temperature explain canopy phenology and onset of spring in a semiarid Steppe. *Great Plains Research*, 25, 121– 138. https://doi.org/10.1353/gpr.2015.0027

Mueller, B., & Seneviratne, S. I. (2014). Systematic land climate and evapotranspiration in CMIP4 simulations. *Geophysical Research Letters*, 41, 128– 134. https://doi.org/10.1002/2013GL058055

Murray-Tortarolo, G., Anav, A., Friedlingstein, P., Sitch, S., Piao, S., Zhu, Z., … Zeng, N. (2013). Evaluation of land surface models in reproducing satellite-

derived LAI over the high-latitude Northern Hemisphere. Part I: uncoupled DGVMs. *Remote Sensing*, 5, 4819– 4838. https://doi.org/10.3390/rs5104819

Oberbauer, S. F., Elmendorf, S. C., Troxler, T. G., Hollister, R. D., Rocha, A. V., Bret-Harte, M. S., … Welker, J. M. (2013). Phenological response of tundra plants to background climate variation tested using the International Tundra Experiment. *Philosophical Transactions of the Royal Society, B: Biological Sciences*, 368. 20120481. https://doi.org/10.1098/rstb.2012.0481

Oleson, K. W., Lawrence, D. M., Bonan, G. B., Flanner, M. G., Kluzek, E., Lawrence, P. J., … Thornton, P. E. (2010). Technical Description of version 4.0 of the Community Land Model (CLM). NCAR Technical Note, NCAR/TN-478 + STR, 257 pp.

Peng, S., Piao, S., Ciais, P., Friedlingstein, P., Zhou, L., & Wang, T. (2013). Change in snow phenology and its potential feedback to temperature in the Northern Hemisphere over the last three decades. *Environmental Research Letters*, 8, 014008. https://doi.org/10.1088/1748-9326/8/1/014008

Piao, S., Fang, J., Zhou, L., Ciais, P., & Zhu, B. (2006). Variations in satellite-derived phenology in China's temperate vegetation. *Global Change Biology*, 12, 672– 685. https://doi.org/10.1111/j.1365-2486.2006.01123.x

Piao, S., Tan, J., Chen, A., Fu, Y. H., Ciais, P., Liu, Q., … Peñuelas, J. (2015). Leaf onset in the northern hemisphere triggered by daytime temperature. *Nature Communications*, 6, 6911. https://doi.org/10.1038/ncomms7911

Pinzon, J. E., & Tucker, C. J. (2014). A non-stationary 1981–2012 AVHRR NDVI3g time series. *Remote Sensing*, 6, 6929– 6960. https://doi.org/10.3390/rs6086929

Polgar, C. A., & Primack, R. B. (2011). Leaf-out phenology of temperate woody plant: from trees to ecosystems. *New Phytologist*, 191, 926– 941. https://doi.org/10.1111/j.1469-8137.2011.03803.x

Poulter, B., MacBean, N., Hartley, A., Khlystova, I., Arino, O., Betts, R., … Peylin, P. (2015). Plant functional type classification for earth system models: results from the European Space Agency's land cover climate change initiative. *Geoscientific Model Development*, 8, 2315– 2328. https://doi.org/10.5194/gmd-8-2315-2015

Richardson, A. D., Anderson, R. S., Arain, M. A., Barr, A. G., Bohrer, G., Chen, G. S., … Xue, Y. K. (2012). Terrestrial biosphere models need better representation of vegetation phenology: results from the North American Carbon Program Site Synthesis. *Global Change Biology*, 18, 566– 584. https://doi.org/10.1111/j.1365-2486.2011.02562.x

Richardson, A. D., Bailey, A. S., Denny, E. G., Martin, C. W., & O'Keefe, J. (2006). Phenology of a northern hardwood forest canopy. *Global Change Biology*, 12, 1174– 1188. https://doi.org/10.1111/j.1365-2486.2006.01164.x

Sacks, W. J., & Kucharik, C. J. (2011). Crop management and phenology trends in the U.S. corn belt: impacts on yields, evapotranspiration and energy balance. *Agricultural and Forest Meteorology*, 151, 882– 894. https://doi.org/10.1016/j.agrformet.2011.02.010

Sarvas, R. (1972). Investigations on the annual cycle of development on forest trees active period. *Communicationes Instituti Forestalis Fenniae*, 886, 76– 110.

Sato, H., Itoh, A., & Kohyama, T. (2007). SEIB-DGVM: A new dynamic global vegetation model using a spatially explicit individual-based approach. *Ecological Modelling*, 200, 279– 307.

Settele, J., Scholes, R., Betts, R., Bunn, S., Leadley, P., Nepstad, D., … Taboada, M. A. (2014). Terrestrial and inland water systems. In C. B Field (Eds.), *Climate Change 2014: Impacts, Adaptation, and Vulnerability. Part A: Global and Sectoral Aspects*. Contribution of Working Group II to the Fifth Assessment Report of the Intergovernmental Panel on Climate Change (pp. 271– 359). Cambridge, United Kingdom and New York, NY: Cambridge University Press.

Seghieri, J., Carreau, J., Boulain, N., De Rosnay, P., Arjounin, M., & Timouk, F. (2012). Is water availability really the main environmental factor controlling the phenology of woody vegetation in the central Sahel? *Plant Ecology*, 213, 861– 870.

Shen, M., Cong, N., & Cao, R. (2015). Temperature sensitivity as an explanation of the latitudinal pattern of green-up date trend in northern Hemisphere vegetation during 1982–2008. *International Journal of Climatology*, 35, 3707– 3712. https://doi.org/10.1002/joc.4227

Shen, M., Piao, S., Chen, X., An, S., Fu, Y. H., Wang, S., … Janssens, I. A. (2016). Strong impacts of daily minimum temperature on the green-up date and summer greenness of the Tibetan Plateau. *Global Change Biology*, 22, 3057– 3066. https://doi.org/10.1111/gcb.13301

Shen, M., Tang, Y., Chen, J., Yang, X., Wang, C., Cui, X., … Cong, N. (2014). Earlier-Season Vegetation Has Greater Temperature Sensitivity of Spring Phenology in Northern Hemisphere. *PLoS ONE*, 9(2), e88178. https://doi.org/10.1371/journal.pone.0088178

Shen, M., Tang, Y., Chen, J., Zhu, X., & Zheng, Y. (2011). Influences of temperature and precipitation before the growing season on spring phenology in grasslands of the central and eastern Qinghai-Tibetan Plateau. *Agricultural and Forest Meteorology*, 151, 1711– 1722. https://doi.org/10.1016/j.agrformet.2011.07.003

Shen, M., Zhang, G., Cong, N., Wang, S., Kong, W., & Piao, S. (2014). Increasing altitudinal gradient of spring vegetation phenology during the last decade on the Qinghai-Tibetan Plateau. *Agricultural and Forest Meteorology*, 189–190, 71– 80. https://doi.org/10.1016/j.agrformet.2014.01.003

Shutova, E., Wielgolaski, F. E., Karlsen, S. R., Makarova, O., Berlina, N., Filimonova, T., … Høgda, K. A. (2006). Growing seasons of Nordic mountain birch in northernmost Europe as indicated by long-term field studies and analyses of satellite images. *International Journal of Biometeorology*, 51, 155– 166. https://doi.org/10.1007/s00484-006-0042-y

Sitch, S., Huntingford, C., Gedney, N., Levy, P. E., Lomas, M., Piao, S. L., … Woodward, F. I. (2008). Evaluation of the terrestrial carbon cycle, future plant geography and climate-carbon cycle feedbacks using five dynamic global vegetation models (DGVMs). *Global Change Biology*, 14, 2015– 2039. https://doi.org/10.1111/j.1365-2486.2008.01626.x

Sitch, S., Smith, B., Prentice, I. C., Arneth, A., Bondeau, A., Cramer, W., … Venevsky, S. (2003). Evaluation of ecosystem dynamics, plant geography and terrestrial carbon cycling in the LPJ dynamic global vegetation model. *Global Change Biology*, 9, 161– 185. https://doi.org/10.1046/j.1365-2486.2003.00569.x

Small, D., Islam, S., & Vogel, R. M. (2006). Trends in precipitation and streamflow in the eastern U. S.: Paradox or perception? *Geophysical Research Letters*, 33, L03403. https://doi.org/10.1029/2005GL024995

S. Solomon, D. Qin, M. Manning, Z. Chen, M. Marquis, K. B. Averyt, … H. L. Miller (Eds.) (2007). *Climate Change 2007—The Physical Science Basis: Working Group I Contribution to the Fourth Assessment Report of the IPCC* (Vol. 4, 996 pp.). Cambridge, United Kingdom and New York, NY: Cambridge University Press.

Stöckli, R., & Vidale, P. L. (2004). European plant phenology and climate as seen in a 20 year AVHRR land-surface parameter dataset. *International Journal of Remote Sensing*, 25, 3303– 3330. https://doi.org/10.1080/0143116031000161814 9

Taylor, K. E., Stouffer, R. J., & Meehl, G. A. (2012). An overview of CMIP5 and the experiment design. *Bulletin of the American Meteorological Society*. https://doi.org/10.1175/BAMS-D-11-00094.1

Thompson, R., & Clark, R. M. (2008). Is spring starting earlier? *Holocene*, 18, 95– 104. https://doi.org/10.1177/0959683607085599

Valliyodan, B., & Nguyen, H. T. (2006). Understanding regulatory networks and engineering for enhanced drought tolerance in plants. *Current Opinion in Plant Biology*, 9, 189– 195. https://doi.org/10.1016/j.pbi.2006.01.019

Vicente-Serrano, S. M., Gouveia, C., Camarero, J. J., Beguería, S., Trigo, R., López-Moreno, J. I., … Sanchez-Lorenzo, A. (2013). Response of vegetation to drought time-scale across global land biomes. *Proceedings of the National Academy of Sciences of the United States of America*, 110, 52– 57. https://doi.org/10.1073/pnas.1207068110

Vitasse, Y., Delzon, S., Dufrene, E., Pontailler, Y.-J., Louvet, J.-M., Kremer, J. A., & Michalet, R. (2009). Leaf phenology sensitivity to temperature in

European trees: do within species populations exhibit similar responses? *Agricultural and Forest Meteorology*, 149, 735– 744. https://doi.org/10.1016/j.agrformet.2008.10.019

Volodin, E. M., & Lykossov, V. N. (1998). Parameterization of heat and moisture transfer in the soil-vegetation system for use in atmospheric general circulation models: 1. Formulation and simulations based on local observation data. *Izvestiya Atmospheric and Oceanic Physics*, 34, 405– 416.

Wang, Q., Adiku, S., Tenhunen, J., & Granier, A. (2005). On the relationship of NDVI with leaf area index in a deciduous forest site. *Remote Sensing of Environment*, 94, 244– 255. https://doi.org/10.1016/j.rse.2004.10.006

White, M. A., Thornton, P. E., & Running, S. W. (1997). A continental phenology model for monitoring vegetation responses to interannual climatic variability. *Global Biogeochemical Cycles*, 11, 217– 234.

Wipf, S., Rixen, C., & Mulder, C. P. H. (2006). Advanced snowmelt causes shift towards positive neighbor interactions in a subarctic tundra community. *Global Change Biology*, 12, 1496– 1506. https://doi.org/10.1111/j.1365-2486.2006.01185.x

Yu, F., Price, K. P., Ellis, J., & Shi, P. (2003). Response of seasonal vegetation development to climatic variations in eastern central Asia. *Remote Sensing of Environment*, 87, 42– 54. https://doi.org/10.1016/S0034-4257(03)00144-5

Yu, H., Luedeling, E., & Xu, J. (2010). Winter and spring warming result in delayed spring phenology on the Tibetan Plateau. *Proceedings of the National Academy of Sciences of the United States of America*, 107, 22,151– 22,156. https://doi.org/10.1073/pnas.1012490107

Yuan, S., & Quiring, S. M. (2017). Evaluation of soil moisture in CMIP5 simulations over the contiguous United States using in situ and satellite observations. *Hydrology and Earth System Sciences*, 21, 2203– 2218. https://doi.org/10.5194/hess-21-2203-2017

Zeng, H., Jia, G., & Forbes, B. C. (2013). Shifts in Arctic phenology in response to climate and anthropogenic factors as detected from multiple satellite time series. *Environmental Research Letters*, 8, 035036. https://doi.org/10.1088/1748-9326/8/3/035036

Zeng, X., Shaikh, M., Dai, Y., Dickinson, R. E., & Myneni, R. B. (2002). Coupling of the Common Land Model to the NCAR Community Climate Model. *Journal of Climate*, 14, 1832– 1854.

Zhang, G., Zhang, Y., Dong, J., & Xiao, X. (2013). Green-up dates in the Tibetan Plateau have continuously advanced from 1982 to 2011. *Proceedings of the National Academy of Sciences of the United States of America*, 110, 4309– 4314. https://doi.org/10.1073/pnas.1210423110

Zhang, H., & Oweis, T. (1999). Water-yield relations and optimal irrigation scheduling of wheat in the Mediterranean region. *Agricultural Water Management*, 38, 195– 211. https://doi.org/10.1016/S0378-3774(98)00069-9

Zhang, X., Friedl, M. A., Schaaf, C. B., Strahler, A. H., Hodges, J. C. F., Gao, F., … Huete, A. (2003). Monitoring vegetation phenology using MODIS. *Remote Sensing of Environment*, 84, 471– 475. https://doi.org/10.1016/S0034-4257(02)00135-9